



Citation for published version:

Whiteside, A, Fisher, CAJ, Parker, SC & Islam, S 2014, 'Particle shapes and surface structures of olivine NaFePO₄ in comparison to LiFePO₄', *Physical Chemistry Chemical Physics*, vol. 16, no. 39, pp. 21788-21794. <https://doi.org/10.1039/c4cp02356k>

DOI:

[10.1039/c4cp02356k](https://doi.org/10.1039/c4cp02356k)

Publication date:

2014

Document Version

Peer reviewed version

[Link to publication](#)

University of Bath

Alternative formats

If you require this document in an alternative format, please contact:
openaccess@bath.ac.uk

General rights

Copyright and moral rights for the publications made accessible in the public portal are retained by the authors and/or other copyright owners and it is a condition of accessing publications that users recognise and abide by the legal requirements associated with these rights.

Take down policy

If you believe that this document breaches copyright please contact us providing details, and we will remove access to the work immediately and investigate your claim.

Particle shapes and surface structures of olivine NaFePO₄ in comparison to LiFePO₄

Alexander Whiteside,^a Craig A. J. Fisher,^b Stephen C. Parker,^a M. Saiful Islam^{a*}

Received (in XXX, XXX) 1st January 2007, Accepted 1st January 2007

⁵ First published on the web 1st January 2007

DOI: 10.1039/b000000x

The expansion of batteries into electric vehicle and grid storage applications has driven the development of new battery materials and chemistries, such as olivine phosphate cathodes and sodium-ion batteries. Here we present atomistic simulations of the surfaces of olivine-structured NaFePO₄ as a sodium-ion battery cathode, and discuss differences in its morphology compared to the lithium analogue LiFePO₄. The calculated equilibrium morphology is mostly isometric in appearance, with (010), (201) and (011) faces dominant. Exposure of the (010) surface is vital because it is normal to the one-dimensional ion-conduction pathway. Platelet and cube-like shapes observed by previous microscopy studies are reproduced by adjusting surface energies. The results indicate that a variety of (nano)particle morphologies can be achieved by tuning surface stabilities, which depend on synthesis methods and solvent conditions, and will be important in optimising electrochemical performance.

1. Introduction

Lithium-ion batteries based on the LiCoO₂ cathode and graphite anode dominate energy storage in portable electronics. However, alternative cathodes are being sought for large-scale applications such as electric vehicles and grid storage.¹ Olivine-structured LiFePO₄ has shown great success and is now produced commercially; it is stable to high temperatures and contains environmentally benign, inexpensive elements.²

Lithium conduction in LiFePO₄ is one-dimensional along [010] channels³⁻⁶, which could be blocked by Fe/Li antisite defects with low formation energies.⁷⁻¹¹ Reducing particle sizes to the nanometre scale counteracts this by reducing migration path lengths.^{12,13} The most desirable morphologies are platelet-shaped with a large (010) face bounded by thin edge surfaces.^{14,15} The large exposed (010) surface allows easy diffusion of Li⁺ into and out of the channels, and the thinness of the platelets reduces the ion-diffusion distance and the impact of an antisite defect blocking any given channel. Numerous studies on LiFePO₄ have shown that such particles and other nanostructures can be created by various hydrothermal and solvothermal routes.¹³⁻²³

Sodium-ion batteries were long overshadowed by the high performance of the lithium-ion battery, but have returned to prominence in applications more sensitive to cost issues and less demanding in energy and power density, for example grid storage.²⁴⁻³¹ Many sodium-ion battery materials are sodium analogues of lithium-ion materials, including the olivine-structured NaFePO₄.³²⁻⁴³

Olivine-structured LiFePO₄ and NaFePO₄ both have high voltages versus the alkali metal, 3.5 V and 2.8 V, respectively, and comparable theoretical specific capacities of 170 mAh g⁻¹ and 154 mAh g⁻¹, respectively.^{3,33,38,39} However, NaFePO₄ does not support high charge/discharge rates; at low rates of C/20 or C/10, the capacity reaches 100 mAh g⁻¹.^{33-35,40} Tripathi *et al.* have suggested that the Na-ion migration energy in NaFePO₄ is lower than the Li-ion migration energy in LiFePO₄, but the Na/Fe antisite defect is even lower in

energy than the Li/Fe defect, implying a greater concentration and therefore more blocked diffusion channels.³⁶

Given that the impact of these antisite defects is controlled by the number and length of the channels, it is important to understand the particle morphologies of NaFePO₄. In this study, the structures and energies of the surfaces of olivine-structured NaFePO₄ were calculated and used to predict the equilibrium particle morphology. By contrasting these results with those for LiFePO₄, the influence of using sodium in place of lithium was assessed.

These results are of particular importance given that olivine-structured NaFePO₄ is metastable with respect to maricite-structured NaFePO₄, a material which is essentially electrochemically inactive.^{35,44} To date, olivine-structured NaFePO₄ has been synthesised by the chemical or electrochemical delithiation of LiFePO₄ to FePO₄, followed by electrochemical sodiation.^{32-35,39-41} The resulting NaFePO₄ particles retain the LiFePO₄ morphology. Our results should therefore indicate whether directly-synthesised olivine NaFePO₄ nanoparticles would have superior properties to those created by electrochemical substitution of Na⁺ for Li⁺.

2. Methods

The overall methodology used in this work has been described in detail in previous publications^{28,45,46}. Potentials-based methods of this type have been applied successfully to a wide range of oxide and phosphate surfaces, including those of lithium battery materials.⁴⁶

The materials were described by the Born model, in which the Coulomb interaction between ions was supplemented by a Buckingham potential, which includes terms for both Pauli repulsion and attractive van der Waals interactions. The iron cations were allowed to polarise through the addition of a shell model. A three-body term was also included to take account of the angle-dependent nature of the PO₄³⁻ tetrahedral units.

The set of interatomic potential and shell model parameters developed in our previous LiFePO₄ study accurately reproduces the orthorhombic structure of bulk LiFePO₄ (space

group *Pnma*), and the corresponding Fe, P, and O parameters were carried into this study. For NaFePO₄, an Na-O Buckingham potential was fitted to the experimental NaFePO₄ olivine structure reported by Moreau *et al.*³⁹. The potential parameters are provided as supplementary information (Table S1).

To model surfaces, 2D periodic boundary conditions were applied to a slab of crystal running parallel to the plane of interest. The surfaces were not considered as simple terminations of the bulk lattice. Instead, the slab was split into two regions; atoms of the upper region (region 1) were relaxed to mechanical equilibrium, while those in the lower region (region 2) were held fixed at their bulk positions. The sizes of the two regions were converged with respect to relaxation of the surface ions and the surface energy (approximately 200 to 500 ions).

The METADISE package⁴⁷ was used for bulk and surface energy calculations and structure optimisations, and VESTA⁴⁸ for visualizing the resulting structures. The advantage of interatomic potential methods has been demonstrated here by the large number of different surface planes and terminations that can be examined individually, quickly and efficiently.

3. Results and discussion

3.1. Bulk crystal properties and surface structures

The potentials developed for this study accurately reproduce the bulk crystal structures of LiFePO₄ and NaFePO₄. A comparison between the calculated unit-cell parameters using our potentials and those determined by experiment are given in Table 1. Similarly, Table 2 compares representative bond lengths in the two materials. The calculated unit cell parameters deviate from the experimental values by at most 0.09 Å, and in most cases by much less; Na-O, Fe-O, and P-O bond lengths have mean deviations of less than 0.004 Å, 0.036 Å, and 0.015 Å, respectively. Reproduction of the relatively complex structure gives us confidence that the interatomic potential model can be used reliably in subsequent calculations.

Table 1: Comparison of calculated and experimental unit cell parameters of NaFePO₄ and LiFePO₄.

Parameter	NaFePO ₄		LiFePO ₄	
	Calc./Å	Expt. ³⁹ /Å	Calc./Å	Expt. ⁴⁹ /Å
<i>a</i>	10.3164	10.4063	10.3713	10.3377
<i>b</i>	6.1638	6.2187	6.0216	6.0112
<i>c</i>	4.9263	4.9569	4.6695	4.6950

Table 2: Comparison of calculated and experimental mean bond lengths of NaFePO₄ and LiFePO₄.

Bond	NaFePO ₄		LiFePO ₄		
	Calc./Å	Expt. ³⁹ /Å	Calc./Å	Expt. ⁴⁹ /Å	
Na-O	2.348	2.344	Li-O	2.176	2.151
Fe-O	2.149	2.185	Fe-O	2.139	2.157
P-O	1.552	1.537	P-O	1.552	1.545

For each material, nineteen possible unique surfaces with indexes less than or equal to two were investigated. For each

surface, all possible terminations were evaluated with the constraint that they were stoichiometric, had zero dipole moment normal to the surface (reconstructing the surface if necessary), and the phosphorus-oxygen bonds were kept intact (due to the high bond energy). The energy of the most stable termination of each surface is reported in Table 3. Note that the energies, and their ranking after relaxation, are quite different from those before relaxation (Table S2), demonstrating that simple bulk terminations are poor models for surface behaviour.

The preferred surface terminations were classified by the scheme of Tasker⁵⁰ into type II surfaces with zero net dipole moment, and type III surfaces with a nonzero net dipole moment in their ‘as-cut’ forms. The type III terminations were reconstructed to eliminate the dipole moment, in most cases by transfer of one or two alkali metal ions to the opposite face of the slab (introducing a vacancy). Unlike LiFePO₄, many of the low-energy surfaces of NaFePO₄ are type II rather than type III (Table S3).

Table 3: Energies of low-index surfaces of NaFePO₄ after relaxation.

Surface	Tasker classification	Surface energy, $E_{\text{surface}} / \text{Jm}^{-2}$
(010)	III	0.52
(110)	II	0.54
(221)	II	0.58
(120)	III	0.59
(021)	II	0.62
(201)	III	0.63
(211)	III	0.63
(011)	III	0.64
(210)	III	0.68
(111)	III	0.68
(100)	III	0.68
(101)	III	0.74
(121)	II	0.70
(212)	III	0.75
(012)	II	0.77
(112)	III	0.79
(122)	II	0.81
(102)	III	0.82
(001)	III	0.90

In general, the surface terminations are atomically rough owing to the presence of intact phosphate tetrahedra. Upon relaxation the framework of FeO₆ octahedra and PO₄ tetrahedra remains quite rigid and the polyhedra only move slightly, normal to the surface: Fe²⁺ moves on the order of 0.2 Å into the bulk and PO₄ groups move on the order of 0.2 Å out of the bulk. By contrast the alkali metal cations relax quite freely. Lithium ions relax into the bulk and sodium ions out of the bulk by 0.1-0.5 Å. The alkali cations in most cases move across the surface towards undercoordinated surface PO₄ groups and away from undercoordinated Fe²⁺-centred polyhedra (FeO₄, FeO₅, *etc.*).

Having described the general trends in surface structure and relaxation, in the following subsections we describe the surface structures that are prominent in the simulated morphology of NaFePO₄.

(010) surface. The (010) surface is the most important in these cathode materials, as the plane is normal to the *b*-axis conduction channel. This surface is one of the lowest energy faces in both

LiFePO₄ and NaFePO₄ (Table 3), meaning that the ends of *b*-axis channels will contribute to a large part of the surface area of both morphologies, which is desirable for good performance. As a type III termination is favoured, there is a Li or Na vacancy at the end of the *b*-axis channel (Fig. 1).

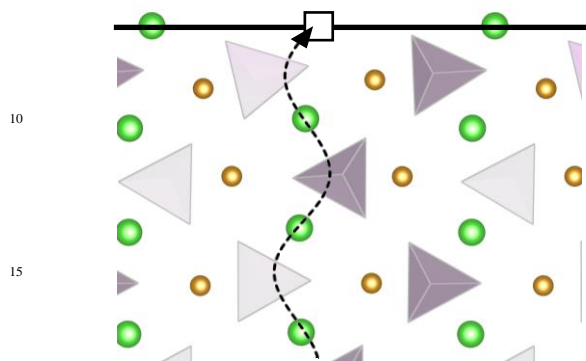


Fig. 1: Schematic side view of the (010) surface of NaFePO₄, showing the sinusoidal Na⁺-migration path (dotted line) to the Na⁺ vacancy (open square), identified from earlier work³⁶, normal to the surface plane. Na⁺: green; Fe²⁺: brown spheres; PO₄³⁻: purple tetrahedra.

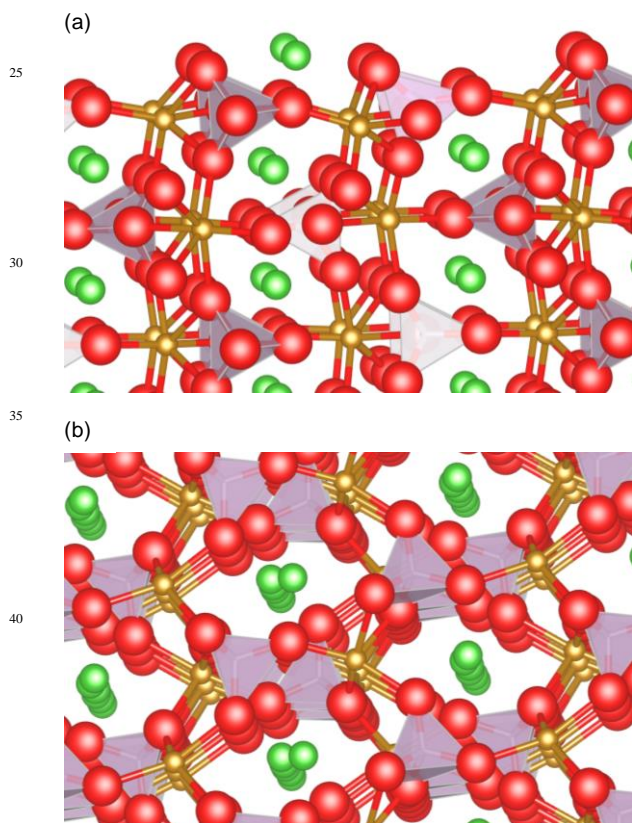


Fig. 2: Relaxed (010) surface of NaFePO₄ in (a) side view and (b) top view. Note relaxation of the undercoordinated Na⁺ at the end of the *b*-axis channel in top view. Na⁺: green; Fe²⁺: brown; P: purple tetrahedra; O: red.

Our previous studies¹¹ found that Na⁺- and Li⁺-ion transport is one-dimensional along the *b*-axis channel in the olivine structure, with the Na⁺ and Li⁺ ions following a curved trajectory between adjacent Na⁺ and Li⁺ sites, respectively.

Tripathi *et al.*³⁶ used potentials-based methods to investigate Na⁺-ion conduction behaviour of olivines NaMPO₄ (*M* = Fe and Mn); the activation energy for Na⁺-ion conduction in NaFePO₄ along the 1D channels in the bulk crystal was reported to be slightly lower than for Li-ion migration in LiFePO₄.³⁶ Their results reveal the crucial importance of the volume-expansion-induced strain during Na⁺ (de)intercalation, which is greater with Na⁺ than Li⁺ for steric reasons, suggesting that materials with a high volume difference between the end-member phases will lead to poor rate capability and faster capacity fade.

We note that Vujkovic *et al.*⁴² have detected faster diffusion of sodium in comparison to lithium from impedance measurements, although Zhu *et al.*³³ have reported the opposite result. In addition, Casas-Cabanas *et al.*³² have reported sodium insertion into FePO₄ via an intermediate phase of approximate composition Na_{2/3}FePO₄ (with Na⁺/vacancy ordering), which may buffer the internal stresses.

(110) surface. The (110) surface is a low energy surface for NaFePO₄ but not LiFePO₄. As this surface exposes the ends of *b*-axis channels, and stabilising it relative to other faces reduces the thickness in the *b* direction, its high stability in NaFePO₄ leads to an improved morphology in terms of alkali-ion insertion and removal.

The improved stability is due to an unusual relaxation in the uppermost part of the surface where a layer “slips” in the (1 10) direction by 1.3 Å (Fig. 3). This widens the normally small *c*-axis channel in the structure, which now contains two sodium ions separated by 4.4 Å. Moving a layer in this way places a sodium ion near the original position of iron, and vice versa. However, this does not block Na migration down the *b*-axis channel, and the expanded *c* channel might even improve ion conduction at the surface. By comparison, the same relaxation in LiFePO₄ involves only small movements of the polyhedra.

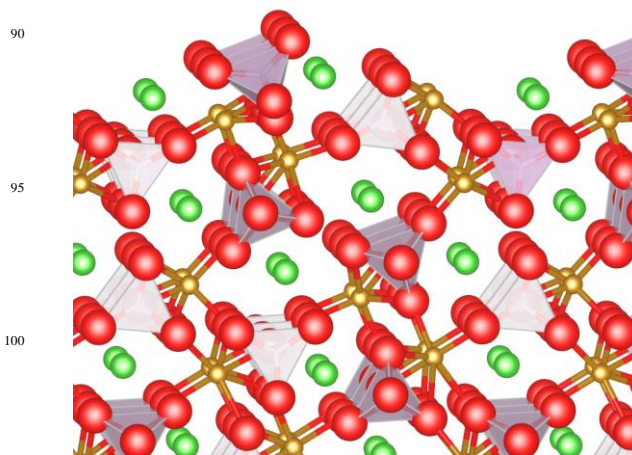


Fig. 3: Side view of relaxed (110) surface of NaFePO₄. Na⁺: green; Fe²⁺: brown; P: purple tetrahedra; O: red.

(201) surface. The (201) surface (Fig. 4) is comparatively unstable in NaFePO₄ due to competition from several low-energy type II surfaces (Table 3); by contrast this surface is relatively low in energy in LiFePO₄. This surface is normal to (010),

making it one of the “edges” of the ideal plate-like morphology. Therefore it is advantageous that this surface is relatively unstable, as it will be less prominent in the NaFePO₄ morphology and lead to wider, thinner particles.

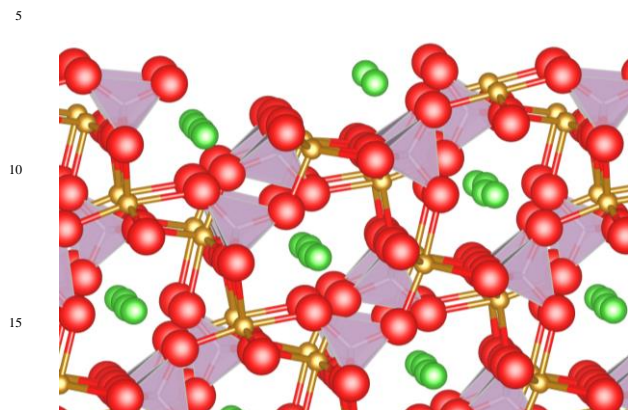


Fig. 4: Side view of relaxed (201) surface of NaFePO₄. Na⁺: green; Fe²⁺: brown; P: purple tetrahedra; O: red

3.2 Particle morphologies

As a result of the relative stabilisation of the (110) surface and the destabilisation of the (201) surface, the equilibrium NaFePO₄ morphology is thinner in the [010] direction and broader in the other directions than the equilibrium LiFePO₄ morphology (Fig. 5). This suggests that directly synthesised NaFePO₄ should exhibit better electrochemical behaviour than particles obtained by ion exchange, which retain the morphology of LiFePO₄. Given that NaFePO₄ forms antisite defects at lower energies (i.e., there will be a higher concentration for the same conditions),³⁶ control of particle morphology is important to offset this disadvantage and improve the material’s performance.

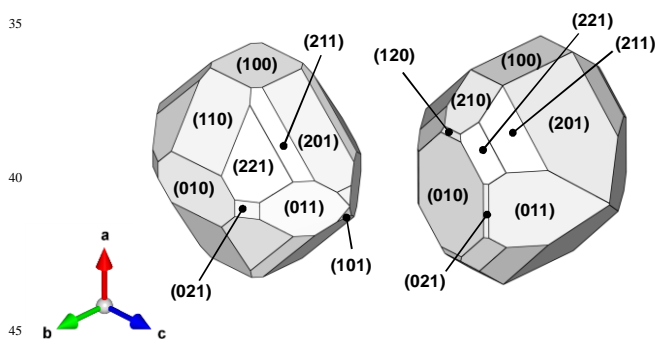


Fig. 5: Predicted equilibrium morphologies of (a) NaFePO₄ and (b) LiFePO₄.

Various synthesis techniques have been developed in the search for high-performance nanoparticles of LiFePO₄, with a wide variety of structures being reported¹³⁻²³. Some electron microscopy examples are shown in Fig. 6 from work of Lu et al²⁰ and Chen et al⁵¹ (also see Table S4). These non-equilibrium morphologies, showing hexagonal-prism, platelet and cube-like shapes, indicate that the relative stabilities of the different facets of the crystals have been altered, for

example, by stabilisation of the (010) face combined with destabilisation of (201).

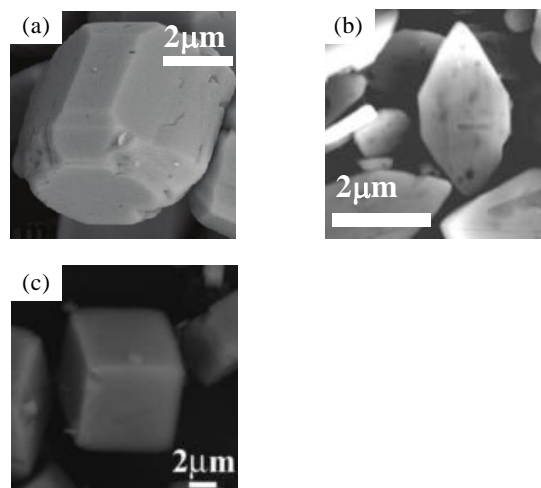


Fig. 6: A variety of LiFePO₄ morphologies observed from experiment: (a) hexagonal-prism-like²⁰, (b) diamond platelet⁵¹, (c) rhombic or cube-like²⁰. Figs 6a and 6c reprinted with permission from ref 20; copyright 2011 American Chemical Society. Fig 6b reprinted with permission from ref 51; copyright 2006 The Electrochemical Society.

By adjusting the surface energies of LiFePO₄ and NaFePO₄ used in computing the Wulff plots of crystal shapes, it is possible to estimate the amount of (de)stabilisation required to create the desirable nanoplate morphology, as shown in Fig. 7. From these diagrams it is clear that the platelike morphology only becomes available when the (010) surface is much more stable with respect to the other surfaces than it is at equilibrium. This result suggests that the surface energy of the (010) plane is greatly reduced (or the surface energies of the other facets greatly increased) during synthetic routes to LiFePO₄ nanoplates.

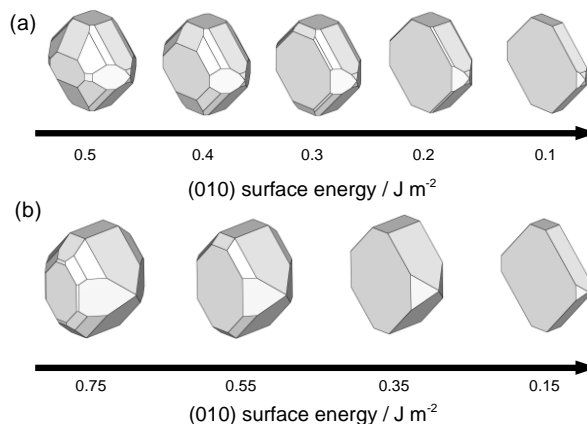


Fig. 7: Variation in the equilibrium morphology of (a) NaFePO₄ and (b) LiFePO₄ with the (010) surface energy, all other surface energies being held constant.

Numerous studies on LiFePO₄ have shown that various particle morphologies, especially the plate-like shapes, can be

prepared.¹³⁻²³ Recent work of Zhao et al²³ reported synthesis of single-crystalline LiFePO₄ nanosheets with highly exposed (010) facets via solvothermal reaction and mechanical exfoliation; such nanosheets provide large surface areas that allow carbon coating and electrolyte penetration to improve electronic conductivity and shorten the lithium-ion diffusion paths. Guo et al²¹ reported a solvothermal route for synthesizing hierarchically-structured LiFePO₄ samples, which were constructed from nanostructured platelets with (010) facets exposed. Other recent studies¹⁹⁻²³ including work of Ma et al²² and Wang et al¹⁹ have shown that particle morphologies and the production of nanoplates are dependent on the solvent composition (e.g. water, ethanol, ethylene glycol, glycerol).

In a similar approach to simulating the plate-like shape, the rhombic or cube-like morphology (Fig 6c) can be achieved by further stabilisation of both the (201) and (010) surfaces, as indicated in Fig. 8. These shapes have been attributed to changes in the growth rates of high-energy facets in the presence of ammonium ions.²⁰ It appears on the basis of these investigations that increased stabilisation of already-low-energy surfaces could also be responsible.

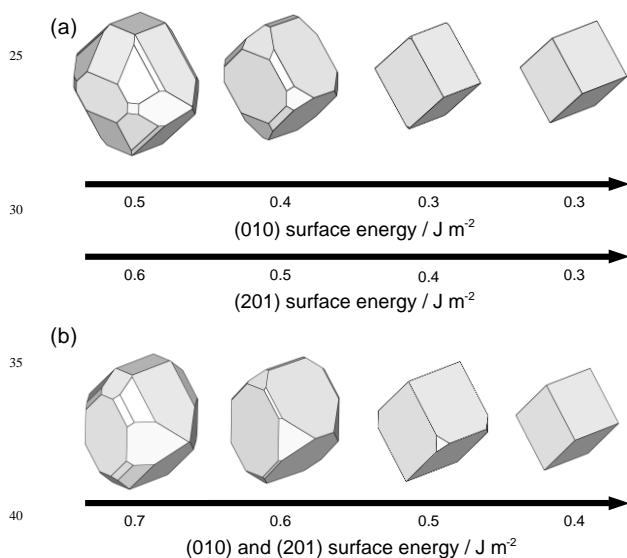


Fig. 8: Variation in the equilibrium morphology of (a) NaFePO₄ and (b) LiFePO₄ with the (010) and (201) surface energies, all other surface energies being held constant.

It is apparent that a variety of particle morphologies can be achieved by manipulating the stabilities of the surfaces expressed in the equilibrium morphology. The strong dependence of the particle morphology on synthesis method and solvent conditions, suggests such effects may be due to increased stability of the surfaces following adsorption of extra-surface species (e.g., solvent molecules, hydroxyl ions). Preliminary analysis of factors such as the number of undercoordinated surface ions and the dipoles at surfaces do not indicate any clear correlations, so that further investigation is needed.

4. Conclusions

The surface structures and equilibrium morphology of olivine NaFePO₄ have been computed and compared with those of LiFePO₄. Similar to LiFePO₄, the surface structures show an uneven topology due to the different sizes of Na⁺, Fe²⁺, and PO₄³⁻ moieties. The calculated equilibrium morphology of NaFePO₄ has an isometric appearance, with several surfaces expressed including (010), (201), (011) and (100).

Despite significant similarities, NaFePO₄ differs from LiFePO₄ in the detail of its surface structures and their relative energies, such that the equilibrium morphology is thinner in the *b*-axis direction. This shorter diffusion path length for sodium ions is important for the rate performance of such a cathode (nano)material.

The prominence of the (010) facet in the morphology is important to the kinetics of Na⁺ extraction/insertion in NaFePO₄-FePO₄, because it is normal to the pathway for sodium-ion conduction. Platelet particles (exhibiting large (010) faces) and cube-like shapes of LiFePO₄ observed by electron microscopy have been reproduced by our simulations. The thinness of the plate-like morphologies parallel to the *b* axis requires the (010) surface to be significantly lower in energy than the other surfaces.

The results presented here confirm that a variety of (nano)particle morphologies can be achieved by tuning the surface stabilities, which depend on the synthesis methods and solvent conditions. Such information will be important in optimising the electrochemical performance of NaFePO₄ and LiFePO₄ cathode materials.

Acknowledgements

We are grateful to the EPSRC for funding (EP/H019596; EP/H003819; EP/L000202/1).

^a Dept of Chemistry, University of Bath, Bath, BA2 7AY, United Kingdom.

⁹⁰ Tel: +44(0)1225 384938. E-mail: m.s.islam@bath.ac.uk

^b Nanostructures Research Laboratory, Japan Fine Ceramics Center, 2-4-1 Mutsuno, Atsuta-ku, Nagoya 456-8587, Japan

[†] Electronic Supplementary Information (ESI) available: Potentials parameters, additional surface plots, additional data on experimental LiFePO₄ morphologies. See DOI: 10.1039/b000000x/

References

1. J. B. Goodenough and K.-S. Park, *J. Am. Chem. Soc.*, 2013, **135**, 1167; C. Masquelier and L. Croguennec, *Chem. Rev.*, 2013, 113, 6552; M. Armand and J.-M. Tarascon, *Nature*, 2008, 451, 652.
2. K. Zaghbi, A. Guerfi, P. Hovington, A. Vijh, M. Trudeau, A. Mauger, J. B. Goodenough and C. M. Julien, *J. Power Sources*, 2013, **232**, 357-369.
3. A. K. Padhi, K. S. Nanjundaswamy and J. B. Goodenough, *J. Electrochem. Soc.*, 1997, **144**, 1188-1194.
4. S. Y. Chung, J. T. Bloking and Y. M. Chiang, *Nat. Mater.*, 2002, **1**, 123-128.
5. Y. G. Wang, P. He and H. S. Zhou, *Energ. Environ. Sci.*, 2011, **4**, 805-817.
6. Z. H. Li, D. M. Zhang and F. X. Yang, *J. Mater. Sci.*, 2009, **44**, 2435-2443.

7. R. Amin, P. Balaya and J. Maier, *Electrochem. Solid-State Lett.*, 2007, **10**, A13-A16.
8. D. Morgan, A. Van der Ven and G. Ceder, *Electrochem. Solid-State Lett.*, 2004, **7**, A30-A32.
9. G. K. P. Dathar, D. Sheppard, K. J. Stevenson and G. Henkelman, *Chem. Mater.*, 2011, **23**, 4032-4037.
10. R. Malik, D. Burch, M. Bazant and G. Ceder, *Nano. Lett.*, 2010, **10**, 4123-4127; R. Malik, A. Abdellahi, G. Ceder, *J. Electrochem. Soc.*, 2013, **160**, A3179-3197.
11. C. A. J. Fisher, V. M. H. Prieto and M. S. Islam, *Chem. Mater.*, 2008, **20**, 5907-5915.
12. C. Delacourt, P. Poizot, S. Levasseur and C. Masquelier, *Electrochem. Solid-State Lett.*, 2006, **9**, A352-A355.
13. C. Delacourt, C. Wurm, P. Reale, M. Morcrette and C. Masquelier, *Solid State Ionics*, 2004, **173**, 113-118; M. Gaberscek, R. Dominko and J. Jamnik, *Electrochem. Commun.*, 2007, **9**, 2778-2783.
14. S. F. Yang, P. Y. Zavalij and M. S. Whittingham, *Electrochem. Commun.*, 2001, **3**, 505-508; J. J. Chen, M. J. Vacchio, S. J. Wang, N. Chernova, P. Y. Zavalij and M. S. Whittingham, *Solid State Ionics*, 2008, **178**, 1676-1693; A.V. Murugan, T. Muraliganth, A. Manthiram, *J. Electrochem. Soc.*, 2009, **156**, A79-A83.
15. S.P Badi, M. Wagemaker, B.L. Ellis, D.P. Singh, W.J.H. Borghols, J.H. Wouter, W.H. Kan, D.H. Ryan, F.M. Mulder, L.F. Nazar, *J. Mater. Chem.*, 2011, **21**, 10085-10093; B. Ellis, W. H. Kan, W. R. M. Makahnouk and L. F. Nazar, *J. Mater. Chem.*, 2007, **17**, 3248-3254; H. Gabrisch, J. Wilcox, M.M. Doeff, *Electrochem. Solid State Lett.*, 2008, **11**, A25-A29.
16. J. M. Tarascon, N. Recham, M. Armand, J. N. Chotard, P. Barpanda, W. Walker and L. Dupont, *Chem. Mater.*, 2010, **22**, 724-739; K. Dokko, S. Koizumi, H. Nakano and K. Kanamura, *J. Mater. Chem.*, 2007, **17**, 4803-4810.
17. X. Qin, X. H. Wang, H. M. Xiang, J. Xie, J. J. Li and Y. C. Zhou, *J. Phys. Chem. C*, 2010, **114**, 16806-16812; W. J. Zhang, *J. Electrochem. Soc.*, 2010, **157**, A1040-A1046; S. Ferrari, R.L. Lavall, D. Capsoni, E. Quartarone, A. Magistris, P. Mustarelli, P. Canton, *J. Phys. Chem. C*, 2010, **114**, 12598-12603; K. Saravanan, P. Balaya, M.V. Reddy, B.V.R. Chowdari, J.J. Vittal, *Energy Environ. Sci.*, 2010, **3**, 457-464.
18. C.M. Julien, A. Mauger, K. Zaghbi, *J. Mater. Chem.*, 2011, **21**, 9955-9968; C.Y. Nan, J. Lu, C. Chen, Q. Peng, Y.D. Li, *J. Mater. Chem.*, 2011, **21**, 9994-9996; J. Lim, V. Mathew, K. Kim, J. Moon, J. Kim, *J. Electrochem. Soc.*, 2011, **158**, A736-A740; U. Boesenberg, F. Meirer, Y.J. Liu, A.K. Shukla, R. Dell'Anna, T. Tylliszczak, G.Y. Chen, J.C. Andrews, T.J. Richardson, R. Kostecki, J. Cabana, *Chem. Mater.*, 2013, **25**, 1664-1672.
19. L. Wang, X.M. He, W.T. Sun, J.L. Wang, Y.D. Li, S.S. Fan, *Nano Lett.*, 2012, **12**, 5632-5636; C. J. Zhang, X. He, Q. S. Kong, H. Li, H. Hu, H. B. Wang, L. Gu, L. Wang, G. L. Cui and L. Q. Chen, *Crystengcomm*, 2012, **14**, 4344-4349; X.Q. Ou, L. Pan, H.C. Gu, Y.C. Wu, J.W. Lu, *J. Mater. Chem.*, 2012, **22**, 9064-9068; X. Qin, J.M. Wang, J. Xie, F.Z. Li, L. Wen, X.H. Wang, *Phys. Chem. Chem. Phys.*, 2012, **14**, 2669-2677; N. Zhou, Y.Y. Liu, J.G. Li, E. Uchaker, S.Q. Liu, K.L. Huang, G.Z. Cao, *J. Power Sources*, 2012, **213**, 100-105; J. Jiang, W. Liu, J.T. Chen, Y.L. Hou, *ACS App. Mater. Interfaces*, 2012, **4**, 3062-3068.
20. Z. G. Lu, H. L. Chen, R. Robert, B. Y. X. Zhu, J. Q. Deng, L. J. Wu, C. Y. Chung and C. P. Grey, *Chem. Mater.*, 2011, **23**, 2848-2859.
21. B.B. Guo, H.C. Ruan, C. Zheng, H.L. Fei, M.D. Wei, *Scientific Rep.*, 2013, **3**, 2788; J.X. Zhu, J. Fiore, D.S. Li, N.M. Kinsinger, Q.Q. Wang, E. DiMasi, J.C. Guo, D. Kisailus, *Crystal Growth Des.*, 2013, **13**, 4659-4666; M. Xie, X.X. Zhang, S.X. Deng, Y.Z. Wang, H. Wang, J.B. Liu, H. Yan, J. Laakso, E. Levanen, *RSC Adv.*, 2013, **3**, 12786-12793.
22. Z.P. Ma, G.J. Shao, Y.Q. Fan, G.L. Wang, J.J. Song, T.T. Liu, *ACS App. Mater. Interfaces*, 2014, **6**, 9236-9244; M.M. Chen, Q.Q. Ma, C.Y. Wang, X. Sun, L.Q. Wang, C. Zhang, *J. Power Sources*, 2014, **263**, 268-275.
23. Y. Zhao, L.L. Peng, B.R. Liu, G.H. Yu, *Nano Lett.*, 2014, **14**, 2849-2853; R.G. Mei, X.R. Song, Y.F. Yang, Z.G. An, J.J. Zhang, *RSC Adv.*, 2014, **4**, 5746-5752; N.A. Siddique, A.M. Allen, P.P. Mukherjee, F.Q. Liu, *J. Power Sources*, 2014, **245**, 83-88.
24. S. P. Ong, V. L. Chevrier, G. Hautier, A. Jain, C. Moore, S. Kim, X. H. Ma and G. Ceder, *Energy Environ. Sci.*, 2011, **4**, 3680-3688.
25. B. L. Ellis and L. F. Nazar, *Curr. Opin. Solid State Mater. Sci.*, 2012, **16**, 168-177.
26. M. D. Slater, D. Kim, E. Lee and C. S. Johnson, *Adv. Funct. Mater.*, 2013, **23**, 947-958.
27. S. W. Kim, D. H. Seo, X. H. Ma, G. Ceder and K. Kang, *Adv. Energy Mater.*, 2012, **2**, 710-721.
28. M. S. Islam and C. A. J. Fisher, *Chem. Soc. Rev.*, 2014, **43**, 185-204.
29. J. Xu, D. H. Lee and Y. S. Meng, *Funct. Mater. Lett.*, 2013, **6**.
30. V. Palomares, P. Serras, I. Villaluenga, K. B. Hueso, J. Carretero-Gonzalez and T. Rojo, *Energy Environ. Sci.*, 2012, **5**, 5884-5901.
31. V. Palomares, M. Casas-Cabanas, E. Castillo-Martínez, M. H. Han and T. Rojo, *Energy Environ. Sci.*, 2013, **6**, 2312.
32. M. Casas-Cabanas, V. V. Roddatis, D. Saurel, P. Kubiak, J. Carretero-Gonzalez, V. Palomares, P. Serras and T. Rojo, *J. Mater. Chem.*, 2012, **22**, 17421-17423; M. Galceran, V. Roddatis, F.J. Zuniga, J.M. Perez-Mato, B. Acebedo, R. Arenal, I. Peral, T. Rojo, M. Casas-Cabanas, *Chem. Mater.*, 2014, **26**, 3289-3294; M. Galceran, D. Saurel, B. Acebedo, V.V. Roddatis, E. Martin, T. Rojo, M. Casas-Cabanas, *Phys. Chem. Chem. Phys.*, 2014, **16**, 8837-8842.
33. Y. J. Zhu, Y. H. Xu, Y. H. Liu, C. Luo and C. S. Wang, *Nanoscale*, 2013, **5**, 780-787.
34. J. Trottier, P. Hovington, F. Brochu, I. Rodrigues, K. Zaghbi, A. Mauger and C. M. Julien, *ECS Transactions*, 2011, **35**, 123-128; K. Zaghbi, J. Trottier, P. Hovington, F. Brochu, A. Guerfi, A. Mauger and C. M. Julien, *J. Power Sources*, 2011, **196**, 9612-9617.
35. J.C. Lu, S.C. Chung, S. Nishimura, A. Yamada, *Chem.*

-
- Mater.*, 2013, **25**, 4557-4565.
36. R. Tripathi, S. M. Wood, M. S. Islam and L. F. Nazar, *Energ. Environ. Sci.*, 2013.
37. M. Avdeev, Z. Mohamed, C. D. Ling, J. C. Lu, M. Tamaru, A. Yamada and P. Barpanda, *Inorg. Chem.*, 2013, **52**, 8685-8693.
38. A. S. Andersson, J. O. Thomas, B. Kalska and L. Haggstrom, *Electrochem. Solid-State Lett.*, 2000, **3**, 66-68.
39. P. Moreau, D. Guyomard, J. Gaubicher and F. Boucher, *Chem. Mater.*, 2010, **22**, 4126-4128; J. Gaubicher, F. Boucher, P. Moreau, M. Cuisinier, P. Soudan, E. Elkaim and D. Guyomard, *Electrochem. Commun.*, 2014, **38**, 104-106.
40. S. M. Oh, S. T. Myung, J. Hassoun, B. Scrosati and Y. K. Sun, *Electrochem. Commun.*, 2012, **22**, 149-152.
41. K. T. Lee, T. N. Ramesh, F. Nan, G. Botton and L. F. Nazar, *Chem. Mater.*, 2011, **23**, 3593-3600.
42. M. Vujkovic, S. Mentus, *J. Power Sources*, 2014, **247**, 184-188.
43. N. Wongittharom, T. C. Lee, C. H. Wang, Y. C. Wang and J. K. Chang, *J. Mater. Chem. A*, 2014, **2**, 5655-5661; J. Sugiyama, H. Nozaki, M. Harada, Y. Higuchi, J.H. Brewer, E.J. Ansaldo, G. Kobayashi, R. Kanno, *Phys. Rev. B*, 2014, 014426.
44. A. Sun, F. R. Beck, D. Haynes, J. A. Poston, S. R. Narayanan, P. N. Kumta and A. Manivannan, *Mater. Sci. Eng. B*, 2012, **177**, 1729-1733.
45. C. A. J. Fisher and M. S. Islam, *J. Mater. Chem.*, 2008, **18**, 1209-1215.
46. M. S. Islam, *Philos T R Soc A*, 2010, **368**, 3255-3267.
47. G. W. Watson, E. T. Kelsey, N. H. deLeeuw, D. J. Harris and S. C. Parker, *J. Chem. Soc. Faraday Trans.*, 1996, **92**, 433-438.
48. K. Momma and F. Izumi, *J. Appl. Crystallogr.*, 2011, **44**, 1272-1276.
49. G. Rouse, J. Rodriguez-Carvajal, S. Patoux and C. Masquelier, *Chem. Mater.*, 2003, **15**, 4082-4090.
50. P. W. Tasker, *J. Phys. C: Solid State Phys.*, 1979, **12**, 4977-4984.
51. G. Y. Chen, X. Y. Song and T. J. Richardson, *Electrochem. Solid-State Lett.*, 2006, **9**, A295-A298.